Journal of Power Sources 187 (2009) 318–323

Contents lists available at ScienceDirect

Journal of Power Sources

journal homepage: www.elsevier.com/locate/jpowsour

Improved corrosion resistance and interfacial contact resistance of 316L stainless-steel for proton exchange membrane fuel cell bipolar plates by chromizing surface treatment

S.B. Lee, K.H. Cho, W.G. Lee, H. Jang*

Department of Materials Science and Engineering, College of Engineering, Korea University, 5-1 Anam-dong, Seongbuk-gu, Seoul 136-713, South Korea

ARTICLE INFO

Article history:
Received 27 May 2008
Received in revised form 15 October 2008
Accepted 3 November 2008
Available online 27 November 2008

Keywords:
Bipolar plates
PEMFC
Chromizing
Corrosion
Stainless steel

ABSTRACT

The electrochemical performance and electrical contact resistance of chromized 316 stainless-steel (SS) are investigated under simulated operating condition in a proton-exchange membrane fuel cell (PEMFC). The corrosion resistance of the chromized stainless steel is assessed by potentiodynamic and potentiostatic tests and the interfacial contact resistance (ICR) is examined by measuring the electrical contact resistance as a function of the compaction force. The results show that the chromizing surface treatment improves the corrosion resistance of the stainless steel due to the high-chromium concentration in the diffuse coating layer. On the other hand, the excess Chromium content on the surface increases the contact resistance of the steel plate to a level that is excessively high for commercial applications. This study examines the root cause of the high-contact resistance after chromizing and reports the optimum process to improve the corrosion resistance without sacrificing the ICR by obtaining a chrome carbide on the outer layer.

1. Introduction

Fuel cells capable of converting chemical energy into electrical power through electrochemical reactions have been extensively studied over the past few decades. Fuel cells have many advantages over conventional power generators in terms of efficiency and environmental friendliness. Various types of fuel cell have been developed [1] and some have been successfully used as power sources for various devices, vehicles, and plants. Among them, the proton-exchange membrane fuel cell (PEMFC) has attracted much research attention due to its acceptance as a viable alternative to replace the combustion engine in automobiles and as a residential power generator. This is because can be operated at low temperatures and can produce a higher power density than other types of fuel cell [2].

One of the main obstacles to the widespread use of PEMFCs, is the high-manufacturing cost, which depends strongly on the production cost of the bipolar plate [1,3]. The bipolar plate is a crucial component in the PEMFC that distributes fuel gases and collects current through the stack. Therefore, since the early development the PEMFC, attention has focused on reducing the cost of the bipolar plate.

The prerequisites for a bipolar plate are low-gas permeability, good electrical and thermal conductivity, good machineability, sufficient strength to support the stack, high-corrosion resistance, and a competitive material cost [4,5]. At present, graphite composites are mainly used for bipolar plates for commercial PEMFC and much effort has focused on replacing them with metals and alloys [5]. Among many candidate materials based on metals and alloys, stainless steel has attracted much attention because of its superior physical and mechanical properties and relatively low price [6,7]. Stainless steel is inferior, however, to graphite in terms of interfacial contact resistance (ICR) and contamination of the membrane electrode assembly by metal corrosion, when it is exposed to PEMFC operating conditions [8,9].

In order to circumvent the shortcomings of stainless steel, various surface coating techniques have been performed, e.g., chemical vapour deposition (CVD) [8], physical vapour deposition (PVD) [9], electroplating [10], and nitriding [11]. Among them, pack cementation, which is based on the CVD process, is considered to be an effective surface treatment to improve the corrosion resistance of steel bipolar plates since it produces a uniform diffuse layer on the steel surface and maintains high coherence at the interface between the diffuse layer and the substrate [12–14]. It is reported, however, that the Cr-enriched surface decreases the electrical conductivity and causes a voltage drop at the interfacial contact [15]. Void formation has also been reported after the pack cementation of Cr for an extended period due to the Kirkendall effect [8,16], which is detrimental to the mechanical strength of the thin steel plates [17].

* Corresponding author. Tel.: +82 2 3290 3276; fax: +82 2 928 3584.
E-mail address: hojang@korea.ac.kr (H. Jang).

0378-7753/$ – see front matter © 2008 Elsevier B.V. All rights reserved.
doi:10.1016/j.jpowsour.2008.11.064

In this study, the effects of Cr cementation processes under different conditions are investigated, in order to determine the optimum conditions for producing a Cr-enriched layer on stainless steel with improved corrosion resistance without sacrificing ICR. The root cause of the cementation-induced improvement is discussed based on the results from detailed composition analysis.

2. Experimental details

2.1. Specimen preparation

Austenite stainless steel (316L SS) sheets (1-mm thick) produced by the Hyundai Steel Co. were used for chromizing experiments. The chemical composition of the sheets is given in Table 1. The sheets were cut into small discs of dimension 20 mm × 20 mm × 1 mm, polished with #100, #200, #320 and #600 SiC abrasive paper and then degreased with acetone in an ultrasonic cleaner. Two different chromizing processes (processes I and II), with different powder compositions and heat treatment schedules, were used. The detailed specimen preparation and pack cementation processes for the two chromizing processes are given in Table 2. After chromizing, the cross-section of the specimen was examined with a scanning electron microscope (SEM, Hitachi, S-4300). The concentration profiles of the diffuse coating layer were obtained by means of electron probe X-ray microanalysis (EPMA, JEOL, JXA-8900R), while Auger electron spectroscopy (AES, Physical Electronics, Model PHI 680) was used to confirm the composition of the thin surface layers after chromizing treatment.

2.2. Electrochemical tests

Potentiodynamic and potentiostatic tests were performed to measure the corrosion resistance of the bare and chromized specimens. During the electrochemical tests, a sulfuric acid solution (1 M) at 80 °C was used as an electrolyte to simulate an accelerated PEMFC operating condition. A three-electrode system constituted the corrosion circuit with graphite as a counter electrode, a saturated calomel electrode (SCE) as a reference electrode, and a steel specimen as a working electrode. All potentials are reported with respect to the SCE. In potentiodynamic tests, the potential was varied from −0.35 V to 1.0 V at a scanning rate of 60 mV min^{-1}. In the potentiostatic test, hydrogen gas was purged to the anode at −0.1 V and oxygen gas was purged to the cathode at 0.6 V to simulate PEMFC operating conditions.

Table 1
Chemical composition of stainless steel 316L (wt.%).

C	Cr	Ni	Mo	Mn	Si	P	S	Fe
0.024	16.83	10.62	2.07	1.13	0.56	0.028	0.004	Bal.

Table 2
Chromizing procedures used in this study.

1. Cutting	20 mm × 20 mm × 1 mm
2. Polishing and cleaning	#100–#600 using SiC abrasive paper Ultrasonic cleaner with acetone for 15 min
3. Chromizing condition	Process I: powder mix (Cr (50 wt.%), Al_2O_3 (43 wt.%), NH_4C (7 wt.%)) was ball milled for 10 h and chromized for 2 h 30 min at 1050 °C in Ar atmosphere Process II: powder mix (Cr (25 wt.%), Al_2O_3 (72 wt.%), NH_4C (3 wt.%)) was ball milled for 10 h and chromized for 23 h at 1050 °C in Ar atmosphere

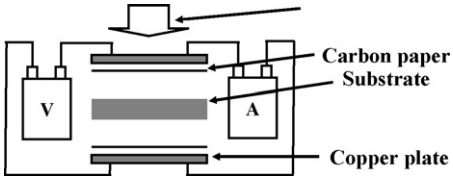

Fig. 1. Schematic of system for measurement of interfacial contact resistance (ICR).

2.3. Interfacial contact resistance (ICR)

The ICR was obtained by measuring the voltage drop across the surface contacts at room temperature. A current of 1 A was applied via two copper plates using a d.c. power supply (Hewlett–Packard) and the voltage drop was measured by means of an Agilent 34401A potentiometer (Fig. 1) [7]. The compaction force was changed from 50 to 500 N cm^{-2} by a push–pull dial gauge (FB-50K, IMADA).

3. Results and discussion

3.1. Microstructure of cemented layer

The microstructure of the diffuse layer after pack cementation was examined with SEM. Micrographs of the cross-sections of the 316L SS plate after cementation using processes I and II (Fig. 2(a) and (b), respectively) is The cross-section of specimen A after process I exhibited three distinct layers: a thin outer layer (about 2 μm thick), a Cr-rich layer (about 30 μm thick), and the substrate. Specimen B after process II, on the other hand, has two layers: a 58-μm thick diffuse coating layer and the substrate. The absence of the thin outer layer and the thicker diffuse layer in Fig. 2(b) are attributed to the longer heat-treatment time of process II. The distribution of Cr in the specimen after the pack cementation processes A and B in Fig. 3, which was mapped using EPMA, also indicates a clear difference in the thickness of the diffuse layers and the existence of the outer layer.

The compositions of Cr, Fe, and Ni were also measured as a function of depth from the surface in specimen A (Fig. 4). Fig. 4 shows the diffuse layer enriched by Cr up to 45 μm and the concentration profile that exhibits a peak on the surface and at the boundary between the diffuse layer and the substrate. The appearance of the two concentration peaks at the heterophase interfaces is attributed to either the segregation of the alloying elements or the formation of a third phase. The composition profiles of specimen B (Fig. 5) are similar to that of specimen A, with local variations of concentrations shown near the boundary between the diffuse layers and the substrate. No concentration peak is found near the surface in the case of specimen B, where as the diffuse layer is extended due to a longer diffusion time. The slight decrease of Ni concentration in the diffuse layer of both specimens is attributed to the phase transformation of the austenite phase to a ferrite phase during cementation because Cr is a ferrite stabilizer [18].

In order to analyze the outer surface layer of specimen A, composition profiles were obtained using AES. The results for the bare specimen (a), specimen A (b), and specimen B (c) are given in Fig. 6. The bare specimen without cementation exhibits high concentrations of carbon and oxygen due to atomic segregation, as described by the Gibbs adsorption isotherm [19]. Specimen B has a higher concentration of oxygen than the bare specimen. This indicates that process II produces an oxide layer that is thickness on the surface than that on the bare specimen [20]. In specimen A, however, only carbon and chrome atoms are detected to a certain depth, which suggests that the outer thin layer after cementation process A is covered with a chrome carbide of composition $Cr_{23}C_6$

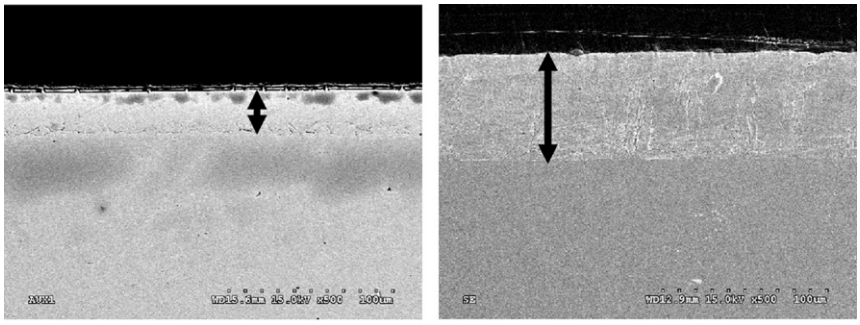

(a) Specimen A (b) Specimen B

Fig. 2. SEM micrographs of cross-section from 316L SS specimens A and B after chromizing processes I and II, respectively. Arrows indicate the depth of cemented layers.

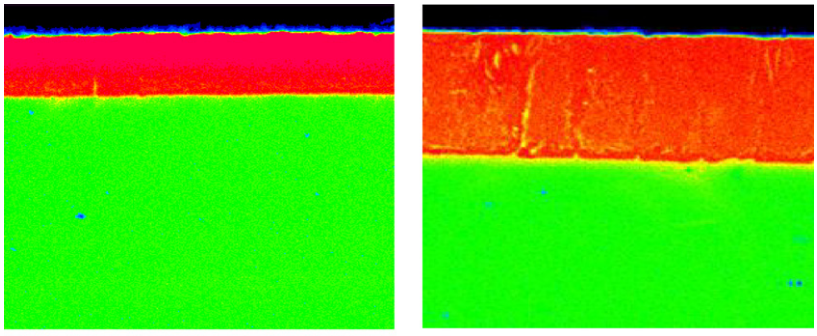

(a) Specimen A (b) Specimen B

Fig. 3. Cr maps of cross-section of (a) specimen A and (b) specimen B after chromizing processes I and II, respectively. Blue, red, and green colors indicate outer surface layer, cemented layer, and SS substrate, respectively. (For interpretation of the references to color in this figure legend, the reader is referred to the web version of the article.)

[8,16]. The chrome carbide layer is removed when the bare specimen is cemented by process II. The disappearance of the chrome carbide layer after chromizing using process II is attributed to the low-Cr content in the powder mix and the long heat treatment time, which prevents carbide formation on the outer surface [17,21].

3.2. Corrosion resistance

The corrosion resistance of 316L SS after cementation was investigated by analyzing the polarization of bare and chromized specimens. The potentiodynamic curves obtained in a simulated PEMFC operating condition are presented in Fig. 7. The potentiodynamic test was carried out in 1 M H_2SO_4 at 80 °C to accelerate the corrosion. Active, passive and transpassive regions are evident in the curves and the chromized specimens exhibit large current density oscillation [8]. The corrosion potential of the bare specimen is −0.26 V (vs. SCE), which is slightly lower than those of the chromized specimens A and B. Exact values of the corrosion potential are not accessible due to the severe oscillation, which is

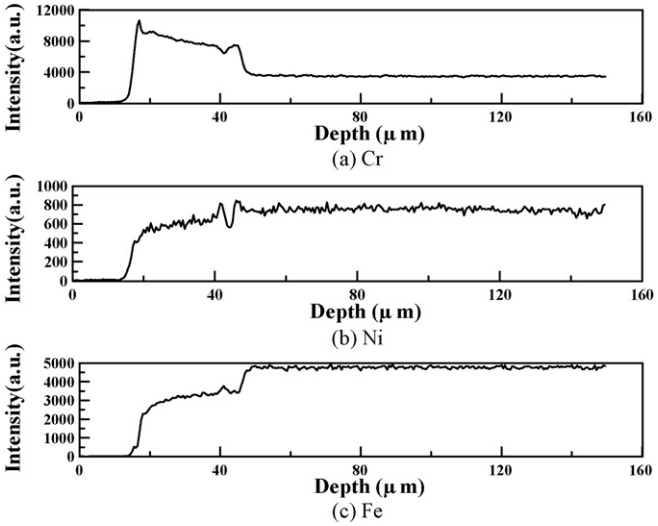

Fig. 4. Concentration profiles of (a) Cr, (b) Ni. and (c) Fe across the Cr-rich layer of specimen A after chromizing process I.

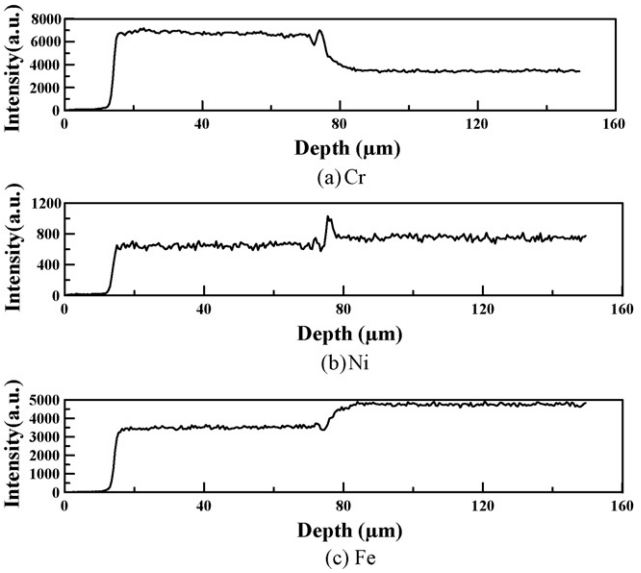

Fig. 5. Concentration profiles of (a) Cr, (b) Ni, and (c) Fe across Cr-rich layer of specimen B after chromizing process II.

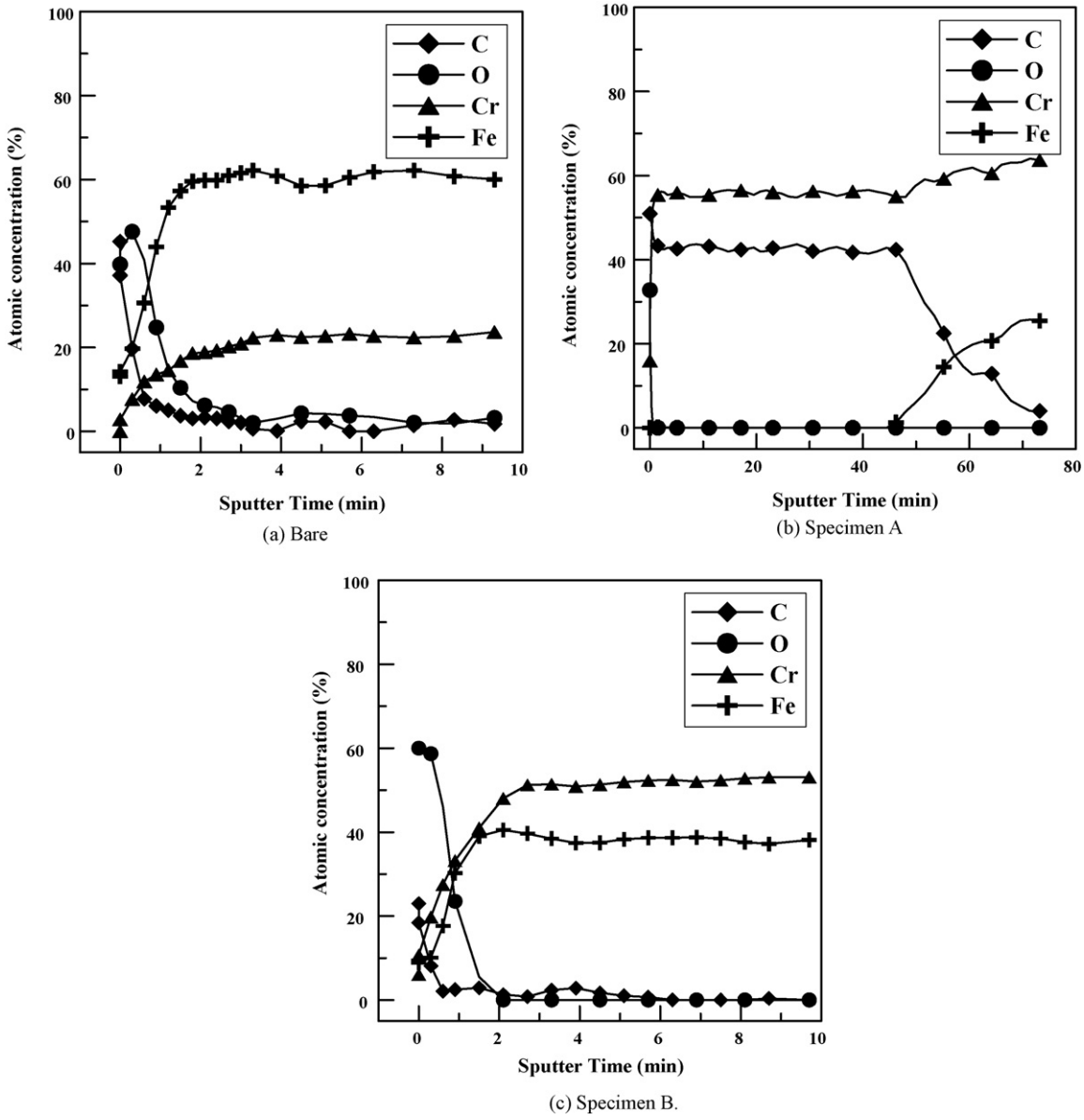

Fig. 6. AES depth profiles of (a) bare specimen, (b) specimen A, and (c) specimen B.

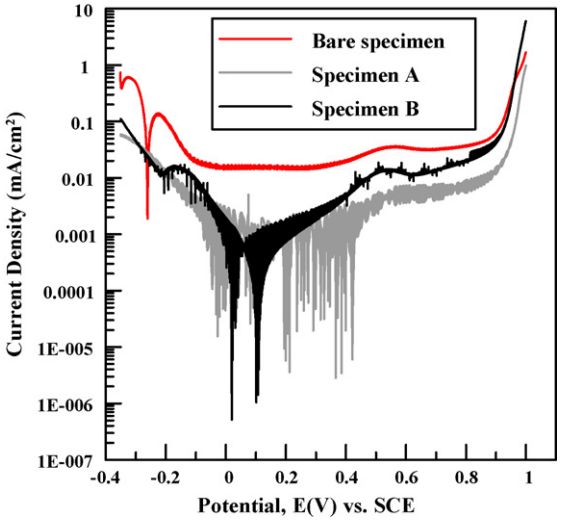

Fig. 7. Potentiodynamic curves obtained from bare specimen, specimen A and specimen B in 1 M H_2SO_4 at 80 °C.

attributed to the build up and breakdown of an oxide layer. Under a simulated PEMFC operating condition of −0.1 V at the anode and 0.6 V at the cathode, the current density is in the following order: bare specimen > specimen B > specimen A. The lower current densities after pack cementation are attributed to the Cr-rich layer on the surface and confirmed that the chromizing processes improves the corrosion resistance of steel bipolar plates during PEMFC operation.

To compare the long-term corrosion resistance of the chromized specimens, potentiostatic tests were performed under a simulated PEMFC operating condition by applying −0.1 V to the anode and 0.6 V to the cathode. The anode was purged with hydrogen gas in a 1 M H_2SO_4 solution at 80 °C, whereas the cathode was purged with oxygen gas in the same electrolyte. Using specimen A, the current densities at the anode and cathode were measured during the potentiostatic test (Fig. 8). The samples exhibit low and stable current densities for an extended period of time that demonstrate the effectiveness of the chromizing processes I and II in improving the corrosion resistance of the stainless steel. Specimen B gives the same level of current density in the anode and cathode during the potentiostatic test.

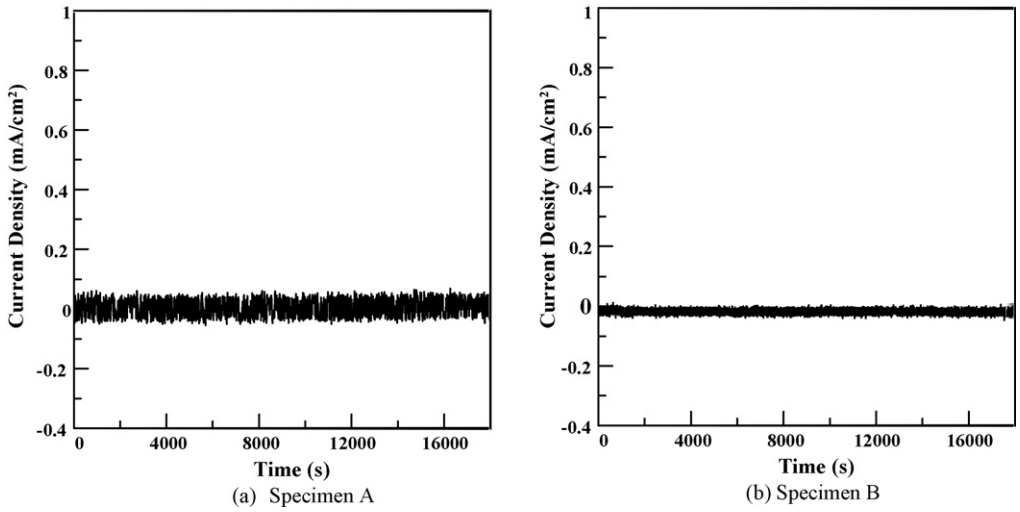

Fig. 8. Potentiostatic curves obtained from (a) specimen A and (b) specimen B at −0.1 V (vs. SCE) with H_2 purging.

3.3. Interfacial contact resistance (ICR)

The electrical conductivity of the bipolar plate is one of the important parameters for PEMFC commercialization because the electrical resistance of the bipolar plate decreases the total voltage obtained when a series of cells are connected in a stack. The electrical resistance at the contact produces a voltage drop and it necessitates more cells to attain a certain voltage. To examine the electrical conductivity of the bipolar plate, ICR is often measured as a function of compaction force [7]. In this study, the range of applied force was 50–500 N cm^{-2}.

Fig. 9 shows the ICR of the three specimens as a function of compaction force. The decrease of ICR with increasing compaction force is attributed to the increased real contact area at high-compaction forces and is closely related to the mechanical properties of the asperities on the surface. The data also reveal that the contact resistance of specimen A is lower than that of the bare specimen and specimen B. The ICR value of the chromized specimen is 19–17 MΩ cm^2 for sample A and 52.5–35.3 MΩ cm^2 for the bare specimen at a compaction force of 100–150 N cm^{-2}. These results show that the chrome carbide on the surface of specimen A reduces the contact resistance, where as the Cr-enriched diffuse layer without carbide layer formation on the surface of specimen B increases the contact resistance to 320.7–233.5 MΩ cm^2 at the same compaction force. The difference in ICR values of bare and specimen B is due to the thicker oxide layer on the surface after process II. This is a salient finding because the low-electrical conductivity has been considered one of the main barriers to the application of stainless steel to bipolar plates, and because it suggests a way to increase the corrosion resistance without sacrificing the ICR.

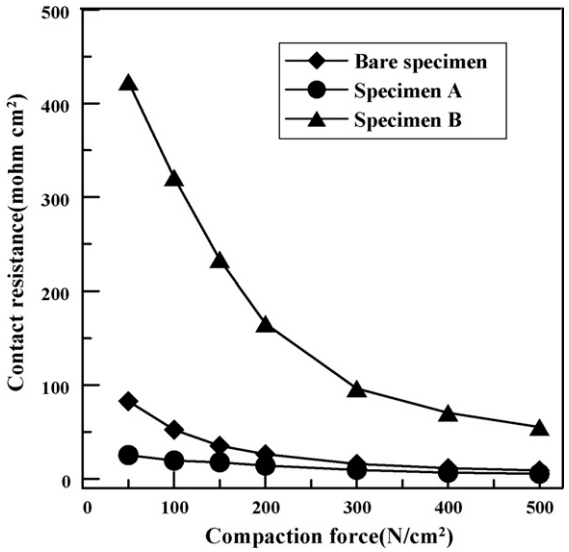

Fig. 9. Interfacial contact resistance of bare specimen, specimen A and specimen B as function of compaction force.

4. Conclusions

The corrosion resistance and ICR of chromized 316L austenitic SS has been examined by using electrochemical tests and by measuring the contact resistance as a function of applied force. The results from the steel specimen chromized with two different processes are as follows:

- Composition analysis shows that the phases formed on the surface of the stainless steel vary according to the chromizing procedure.
- Chromized specimens have improved corrosion resistance in the potentiodynamic and potentiostatic tests.
- The ICR is decreased by the presence of chrome carbide on the outer surface after a chromizing procedure, where as the specimen without the chrome carbide layer exhibits a high ICR.

Acknowledgement

The work was supported by grants from the SEOUL R&BD Program at Korea University.

References

[1] J. Larminie, A. Dicks, Fuel Cell Systems Explained, 2nd ed., John Wiley & Sons Ltd., 2005.
[2] Y. Hung, K.M. El-Khatib, H. Tawfik, J. Power Sources 163 (2006) 509–513.
[3] Y. Wang, D.O. Northwood, Electrochim. Acta 52 (2007) 6793–6798.
[4] M. Ruge, F.N. Buchi, Proceedings of the First European PEFC Forum, 2001, pp. 299–308.
[5] B.D. Cunningham, J. Huang, D.G. Baird, Int. Mater. Rev. 52 (2007) 1–13.
[6] H. Tawfik, Y. Hwang, D. Mahajan, J. Power Sources 163 (2007) 755–767.
[7] H. Wang, M.A. Sweikart, J.A. Turner, J. Power Sources 115 (2003) 243–251.
[8] K.H. Cho, W.G. Lee, S.B. Lee, H. Jang, J. Power Sources 180 (2008) 597–601.
[9] S.J. Lee, C.H. Huang, Y.P. Chen, J. Mater. Process. Technol. 140 (2003) 688–693.
[10] D.G. Nam, H.C. Lee, J. Power Sources 170 (2007) 268–274.
[11] H. Wang, M.P. Brady, K.L. More, H.M. Meyer III, J.A. Turner, J. Power Sources 138 (2004) 79–85.

[12] D.M. Miller, S.C. Kung, S.D. Scarberry, R.A. Rapp, Oxid. Met. 29 (1988) 239–254.
[13] C.J. Kim, H.S. Yun, J. Kor. Inst. Met. 23 (1985) 619–626.
[14] F.D. Geib, R.A. Rapp, Oxid. Met. 40 (1993) 213–228.
[15] H. Wang, J.A. Turner, J. Power Sources 128 (2004) 193–200.
[16] Y.D. Kogan, B.P. Sereda, E.P. Kostogorov, Met. Sci. Heat Treat. 36 (1994) 135–139.
[17] S.K. Kim, W.S. Shin, J. Kor. Inst. Met. Mater. 30 (1992) 1507–1513.
[18] W.F. Smith, Structure and Properties of Engineering Alloys, 2nd ed., MacGraw-Hill, 1993.
[19] H. Butt, K. Graf, M. Kappl, Physics and Chemistry of Interfaces, 2nd ed., Wiley-VCH, 2006.
[20] T. Hirabayashi, Y. Sun, M. Saeki, J. Nucl. Mater. 175 (1990) 177–183.
[21] D.R. Gabe, Principles of Metal Surface Treatment and Protection, Pergamon Press, 1978.